SILICON SENSORS VS. PYRANOMETERS – REVIEW OF DEVIATIONS AND CONVERSION OF MEASURED VALUES

Mariella Rivera, Christian Reise
Fraunhofer Institute for Solar Energy Systems ISE
Heidenhofstrasse 2, 79110 Freiburg, Germany
Phone +49 1520 4030386   mariella.josefina.rivera.aguilar@ise.fraunhofer.de

ABSTRACT: Many steps in a solar energy project — resource assessment, design, yield prediction, operation and maintenance — depend on accurate and reliable solar irradiance measurements. However, different types of sensors are used and have multiple applications, depending on their measurement. We have considered the main two types of sensors: thermal irradiance sensors (pyranometers) and silicon reference cells. In this study, first we present the differences in measurement results of the two sensors. This is accomplished by evaluating the global irradiance in the plane of array (POA) measured from both sensors installed in different photovoltaic systems (PV systems) around Germany. From this assessment, we enumerate the main factors that contribute to their differences: temperature dependence, angular response, spectral response and calibration deviation. Furthermore, a set of correction equations is applied to the silicon reference cell's data. These equations correlate the two sensors and the factors that contribute to their deviation (obtained from the data analysis, previous studies and the sensor's technical specifications). Finally, we evaluate the correction model with a new set of data, achieving a reduction of the differences between sensors (Root Mean Square Deviation RMSD) of around 38%.
Keywords: Monitoring, Reference Cell, Pyranometer, Qualification and Testing

1   INTRODUCTION

The measurement of solar irradiance is the key to a precise assessment of a solar energy project; therefore, there is a necessity for a high-precision sensor to provide such measurements.

There are two categories of instruments that are used for the irradiance measurements: The first is thermal radiation sensors, also known as thermopile pyranometers. They are high precision instruments mostly used in meteorological stations due to their nearly constant spectral sensitivity over the complete solar spectrum. They have a temperature compensation circuit to reduce the error caused by the changes in ambient temperature. However, their response time tends to be relatively slow (up to 15 seconds). This gives them a disadvantage during clear/cloudy day transitions that can lead to significant errors in instantaneous measurements [1]. Measurements performed with a pyranometer are denoted as G_{pyr} throughout this paper.

The second category is photovoltaic radiation sensors, in which photodiode pyranometers and silicon solar cells (reference cells) are used. The latter are an economic alternative for irradiance monitoring. They show a fast time response, which makes them more reliable in case of rapid solar radiation changes. In addition, they have nearly the same spectral sensitivity as the PV modules present in the system. Some problems that might be encountered are the non-uniform spectral response and their thermal dependence [1, 2]. Measurements performed with a reference cell are denoted as G_{si} throughout this paper.

As shown in Figure 1, the irradiance measurements of these two sensors present significant differences. In general, the differences are larger in the early morning and late afternoon due to the flat cover glass of the reference cells; high angles of incidence (AOI) of the sunlight have a greater effect on the reference cells measurements compared to the pyranometer measurements. High AOI increases light reflectance from the sensor's cover (reflection losses) that lowers the measured signal [3].

To have an insight into the factors that contribute to

their differences, data from the year 2017 was gathered from six monitoring systems around Germany. The study works with solar irradiance measured in the plane of array (POA) in five minutes intervals from a thermopile pyranometer CMP11 from Kipp & Zonen and a mono-crystalline silicon sensor from Mencke & Tegtmeyer, with an embedded Pt100 temperature sensor on the rear surface of the cell. From the data analysis and previous studies, it can be observed that the main causes of deviation are the temperature dependence, angular response, spectral response and calibration deviation.
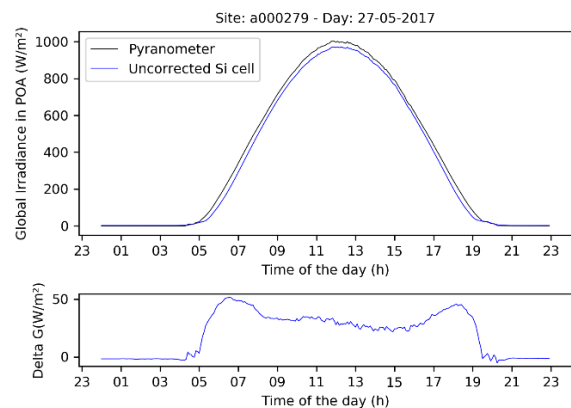
Figure 1: Example of deviations between irradiance measurements. Top graph: global irradiance measurements in POA as recorded by the pyranometer and the reference cell. Bottom graph: the difference between the sensor's readings.

This study aims to analyze the physical properties and design differences between reference cells and thermopile pyranometers, which cause the mismatch measurements between them. Based on this, we create a set of correlations and equations as a model that can correct the reference cell's measurements, to mimic the readings of a high precision thermopile pyranometer. With this model, reference cell's data could be more useful in the different

processes of a solar energy project and uncertainties related to comparisons of both categories of sensors could be reduced [4, 5].

2 METHODOLOGY

2.1 Variables and data filtering

Apart from the measured solar irradiance in POA and cell temperature, new variables are calculated. This establishes the influence of sun position on the measurement difference between the irradiance sensors. Solar position angles and related variables are calculated using pvlib-python, which contains a set of documented functions and classes for the simulation of the performance of photovoltaic energy systems. It considers basic information like the location, time and atmospheric pressure at the site [6]. The new variables comprise zenith, elevation, and azimuth angles, angle of incidence (AOI), air mass (AM) and clear sky irradiance.

To generate the correlation equations between the two sensors and the new calculated variables, which will be used as corrections, a training set of measured data from all the monitoring systems across one year is used. The data is filtered for AOI smaller than 90⁰ to avoid errors in measurements due to distortion and reflection losses. These errors are present mostly in reference cell measurements due to their flat cover glass design [7]. Afterward, the sequence of corrections is applied to irradiance measurements comprising the whole range of solar incident angles during the final model evaluation. In addition, high air mass (AM) values contribute to the distortion of the derived corrections [8]; therefore, the data is filtered for irradiance measurements with an air mass lower than AM10.

$$k = \frac{G_{meas,pyr}}{G_{clearsky}} \qquad (1)$$
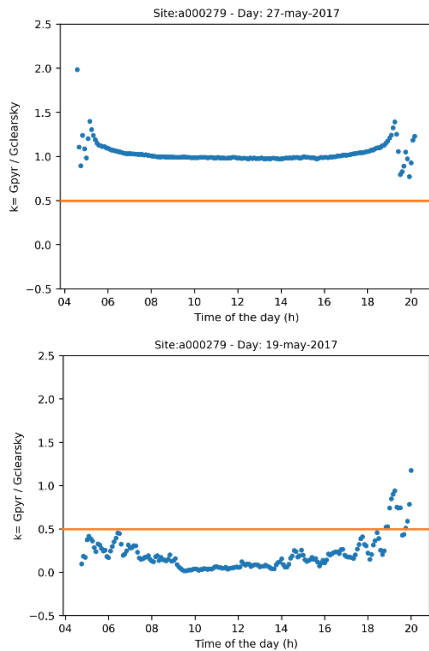
Figure 2: Example of the clear-sky index k for a clear sky day (top graph) and a cloudy sky day (bottom graph).

Another factor for the filtering of the data is the dis-

tinction between clear and cloudy sky days, which is useful when analyzing the difference in measurement behavior between those days. We define the parameter k in equation (1), known as clear-sky index, as the ratio of the irradiance measured with the pyranometer ($G_{meas,pyr}$) and simulated clear sky irradiance in the POA ($G_{clearsky}$) as calculated with the pvlib-python library.

The clear-sky index was computed and plotted for the whole dataset. A threshold value of 0.5 was used to separate clear and cloudy sky days. That means that irradiance measurements with k values bigger than 0.5 are classified as clear sky day values, while those with k values below 0.5 belong to cloudy sky days. Figure 2 shows data for two example days.

2.2 Correction sequence

As an overview, the general correction procedure that has been created starts with a temperature correction to the reference cell's uncorrected irradiance measurements. Afterwards, the model differentiates and separates the data between clear and cloudy sky days. Furthermore, an angular response correction and a spectral response correction are applied to the data. For clear sky days, correction equations given for the specific reference cell, taken from previous studies and technical specifications, are applied. For cloudy sky days, correlation equations found by data analysis and fitted to the tendency of data under cloudy conditions are used. Lastly, the model applies a calibration correction. These steps are explained in detail in the following sections.
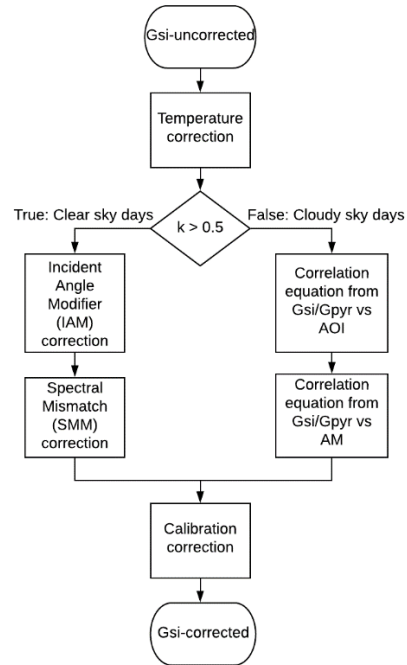
Figure 3: Correction sequence applied to the reference cell's irradiance measurements G$_{si}$.

2.3 Temperature correction

Photovoltaic sensors like reference cells show a linear temperature dependency related to the temperature coefficient of short circuit current [9]. This is considered by the manufacturer, and typically, a correction equation (2) for external temperature compensation is given [10].

$$G_{temp.corr} = G_{uncorr}(1 - \alpha(T_{sensor} - 25°C)) \quad (2)$$

Here, α is the temperature coefficient in 1/°C that is provided from the calibration laboratories at Fraunhofer ISE as 0.00034/°C for this specific sensor model, G_{uncorr} is the reference cell's irradiance measurements without temperature correction and T_{sensor} is the sensor's rear cell surface temperature.

2.4 Angular response correction

The dependency on AOI is one of the main discrepancies between the two categories of sensors since their optical mechanisms are significantly different. The thermopile pyranometer with its glass dome allows a wider response to the sun's relative position, while the reference cell with the flat glass cover presents errors at high AOI due to reflection losses [9]. To correct the deviation of the reference cell's measurements due to the angular response, the model divides the data into clear and cloudy sky days, as the data revealed different behavior in measurements depending on the weather conditions.

For clear sky days, the model applies the values of the Incident Angle Modifier (IAM) curve depending on the AOI, which is provided by the manufacturer [11]. The values in the curve take into account the decrease of irradiance due to reflection on the glass cover of the sensor by the increase of the AOI [12]. It is applied with equation (3).

$$G_{AOIcorr} = \frac{G_{temp.corr}}{IAM} \quad (3)$$

For cloudy sky days, we looked at the correlation between the two sensors and AOI, by plotting the ratio reference cell over pyranometer measured irradiance (Gsi/Gpyr) versus AOI from all the monitoring sites in the year 2017 (Figure 4). By looking for an equation that fits the tendency of data from a cloudy day, the equation (4) is obtained and applied in the model as an angular response correction for cloudy days.

$$G_{AOIcorr} = \frac{G_{temp.corr}}{0.6510 + 0.3092 \ln(AOI) - 0.0820 \ln(AOI)^2 + 0.0066 \ln(AOI)^3} \quad (4)$$
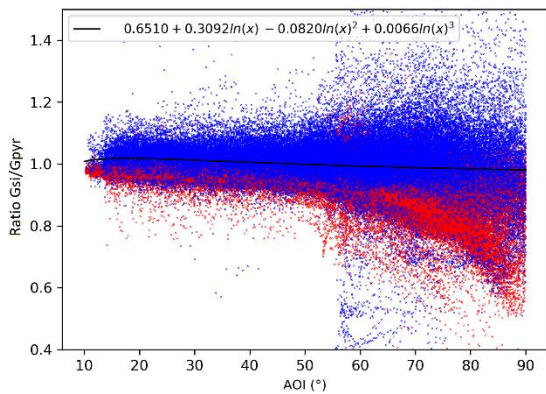
Figure 4: Ratio Gsi / Gpyr vs AOI, for clear sky days (red dots) and cloudy sky days (blue dots). The black line gives the polynomial fit equation to cloudy sky data.

2.5 Spectral response correction

The spectral response refers to how efficient the sensor detects the radiation depending on the wavelength. Thermopile pyranometers have a flat uniform response through the whole wavelength range, whereas the response of reference cells is limited and not uniform [9]. To correct this deviation between the sensors, the model again divides the data into clear and cloudy sky days.

For clear sky days, the values of the Spectral Mismatch Factor (SMM) for this type of reference cell are given by [13], extrapolated up to AM10 and applied as a correction in this model. The SMM quantifies the performance of the sensor when it has been exposed to a spectral irradiance different to the reference spectrum at standard test conditions (STC) as used during the calibration of the sensors. The correction with these values is applied with equation (5).

$$G_{AMcorr} = \frac{G_{AOIcorr}}{SMM} \quad (5)$$

For cloudy sky days, a correlation equation is applied as a correction. By plotting the ratio reference cell over pyranometer measured irradiance (Gsi/Gpyr) versus AM from all the monitoring sites in the year 2017 (Figure 5), a polynomial fitting to the cloudy sky data tendency is obtained, then transformed to a spectral response correction equation for cloudy days (5).

$$G_{AMcorr} = \frac{G_{AOIcorr}}{1.0198 - 0.0266 \ln(AM) + 0.0023 \ln(AM)^2} \quad (5)$$
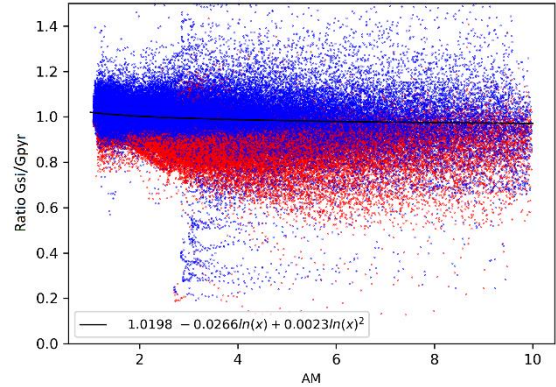
Figure 5: Ratio Gsi / Gpyr vs AM, for clear sky days (red dots) and cloudy sky days (blue dots). The black line gives the polynomial fit equation to cloudy sky data.

2.6 Calibration deviation correction

The calibration of both pyranometers and reference cells is carried out under standard test conditions at a temperature of 25°C, a perpendicular irradiance of 1000 W/m², and under a spectrum corresponding to AM1.5 [14]. Due to this, a way to identify when a sensor has a deviation concerning the calibration factors is to analyze the differences around noontime, when conditions are similar to STC carried out in the calibration procedure. The model filters the data to obtain the difference between the pyranometer and reference cell for clear sky days (k > 0.8), around solar noontime (11:30–13:30) and irradiance values larger than 900 W/m². The average difference from the filtered set of data can be calculated as a percentage (%calib) in equation 6 and then used as a correction factor (equation 7).

$$\%calib = \frac{Average\ irradiance\ dif.\ at\ noon\ time}{Average\ irradiance\ at\ noontime} \quad (6)$$

$$G_{Calib.corr} = G_{AMcorr}(1 + \%calib) \qquad (7)$$

However, if there is no data from a pyranometer as a reference, it has been considered from previous studies [8, 15] an average calibration percentage deviation of 2%, which is applied by the model in equation 7.

3   EVALUATION

With this set of correction equations and sequence of steps, the model was tested (among others) for the same monitoring systems in this study but with data from the following year (2018). The results were obtained by comparing the corrected measurements of the reference cell with the measurements of the pyranometer as a reference for a given monitoring site. Table I shows the average deviation (RMSD) between uncorrected sensor measurements from the complete set of monitoring systems for the year 2018 as 18.83 W/m² (11.82%). After the correction model was applied to the reference cell data, the deviation was reduced to 11.90 W/m² (7.46%), which represents an average decrement of deviations of 37.8% for all the monitoring systems. The table also shows how the RMSD between the pair of sensors was reduced after each correction step.

The results also show how the silicon sensor's irradiance measurements were underestimated compared to the pyranometer measurements (Table II), seen from negative values for mean bias deviation (MBD) before the correction. After the correction procedure, the values of MBD were closer to zero, which indicates the model provides a precise estimation in comparison with the reference measurements.

Table I: Root Mean Square Deviation (RMSD) in W/m² after each correction step and % reduction of the RMSD.

Site	Uncorr.	AOI corr.	AM corr.	Calib. Corr.	%Red.
A000257	19.67	15.17	15.23	12.87	34.6%
A000270	17.12	12.89	12.88	10.84	36.7%
A000272	13.37	9.45	9.25	8.32	37.7%
A000279	16.02	10.73	10.70	7.79	51.4%
A000281	18.60	14.24	14.36	11.70	37.1%
A000302	28.19	23.51	23.54	19.89	29.4%
Average	**18.83**	**14.33**	**14.32**	**11.90**	**37.8%**

Table II: Mean Bias Deviation (MBD) in W/m² before and after the correction procedure.

Site	Uncorrected	Corrected
A000257	−9.48	−2.30
A000270	−6.67	+0.83
A000272	−6.08	+1.16
A000279	−7.53	+0.13
A000281	−9.33	−2.11
A000302	−12.25	−4.42
Average	**−8.56**	**−1.12**

For a single clear sky day from one of the test sites, the effects of the correction steps are presented in Figure 6. The top graph shows the result of the correction steps in dashed lines, which now come closer to the measurements from the pyranometer (black line). The bottom graph shows the difference between sensor measurements (pyranometer – silicon sensor) starting with the difference from the uncorrected reference cell's irradiance measurements (blue line) around 50 W/m². Next, the correction steps are applied (dashed lines), getting closer to a difference of 0 W/m² (red dashed line).
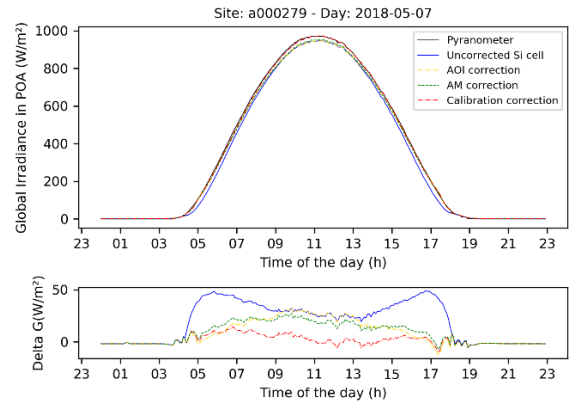
Figure 6: Top graph: global irradiance measurements in POA by both sensors. Bottom graph: the difference between the sensors, before (blue line) and after every correction step (dashed lines).

4   CONCLUSIONS

This study aimed to create a correction model that could be able to reduce the differences between the reference cell and thermopile pyranometer's irradiance measurements. An improvement of the silicon irradiance sensor's data was achieved, which now mimics the behavior of the pyranometer measurements (Figure 7). Based on these results, the silicon irradiance sensor could potentially be used as an economic and high precision alternative in solar energy projects and irradiance monitoring.
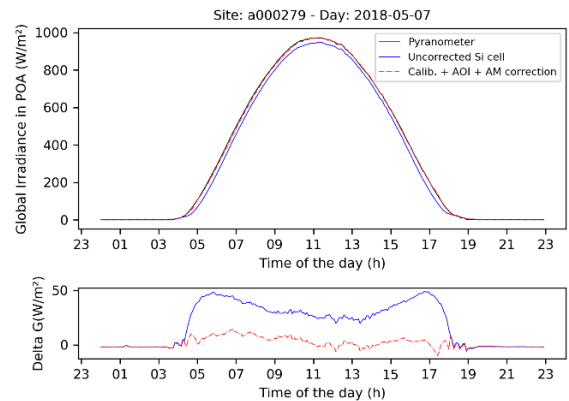
Figure 7: Top graph with the global irradiance measurements in the POA by both sensors and the bottom graph shows the difference between the sensors, before (blue line) and after the correction procedure (red line).

The final model, implemented in Python, requires the location information (latitude, longitude, altitude, tilt angle, azimuth angle), the reference cell's irradiance measurements and device temperature as an input to execute the correction process. It partly eliminates the underestimation of the measurements from the reference cell that now are similar to the readings of the pyranometer for clear and cloudy sky conditions.

5   FURTHER WORK

To improve the model and have a better description of the behavior and deviations from both sensors, a larger set of training data should be considered for the calculation of the correction equations.

For the correction of angular losses, instead of a very general separate treatment of clear and cloudy days, the diffuse fraction or direct to diffuse ratio of the irradiance should be used to calculate a correction for every individual time step. As separate measurements of diffuse irradiance in POA or direct normal irradiance are usually not available, a model such as described in [16] should be used.

An improvement in the calibration correction should be considered. Currently, the model uses an estimated 2% calibration correction factor based on the results from previous studies. Here a more precise value should be used that could consider the correlation between the calibration deviation and the time that has passed since the calibration procedure.

For the spectral response correction, the values of SMM were taken from a previous study. However, tests indicated that site and time specific spectral irradiance data would allow to calculate an SMM that fits the particular measurement and thus can improve the correction and reduce problems like overcorrection.

Lastly, soiling effects could not be analyzed in this study. Further assessment of the irradiance measurements over time and the cleaning processes on a monitoring system, could help to correct the soiling deviation between sensors as a function of the time that has passed after cleaning.

5   ACKNOWLEDGEMENT

6   REFERENCE

[1]   N. Erraissi, N. Aarich, M. Akhsassi, M. Raoufi, and A. Bennouna, "An Inexpensive and Accurate Solar Irradiance Sensor Based in a Small Calibrated PV Module," (eng), *33rd European Photovoltaic Solar Energy Conference and Exhibition*, pp. 1588–1592, Amsterdam, 2017.

[2]   L. Alados-Arboledas, F. J. Batlles, and F. J. Olmo, "Solar radiation resource assessment by means of silicon cells," *Solar Energy*, vol. 54, no. 3, pp. 183–191, 1995.

[3]   Sustainable Technologies Evaluation Program (STEP), "Field Comparison of a Photovoltaic Reference Sensor and a Pyranometer," Renewable Energy: Photovoltaics, 2017. [Online] Available: https://sustainabletechnologies.ca/home/renewable-energy/solar/photovoltaics/field-comparison-photovoltaic-reference-sensor-pyranometer/pvsensor-and-pyranometer-comparison-techbrief/.

[4]   N. H. Reich, B. Mueller, A. Armbruster, W. G. J. H. M. van Sark, K. Kiefer, and C. Reise, "Performance ratio revisited: is PR > 90% realistic?," *Prog. Photovolt: Res. Appl.*, vol. 20, no. 6, pp. 717–726, 2012.

[5]   B. Müller, L. Hardt, A. Armbruster, K. Kiefer, and C. Reise, "Yield Predictions for Photovoltaic Power Plants: Empirical Validation, Recent Advances and Remaining Uncertainties," (eng), pp. 2591–2599, Amsterdam, 2014.

[6]   W. F. Holmgren, C. W. Hansen, and M. A. Mikofski, "pvlib python: a python package for modeling solar energy systems," *JOSS*, vol. 3, no. 29, p. 884, 2018.

[7]   J. J. Michalsky, R. Perez, L. Harrison, and B. A. LeBaron, "Spectral and temperature correction of silicon photovoltaic solar radiation detectors," *Solar Energy*, vol. 47, no. 4, pp. 299–305, 1991.

[8]   J. J. Michalsky, L. Harrison, and B. A. LeBaron, "Empirical radiometric correction of a silicon photodiode rotating shadowband pyranometer," *Solar Energy*, vol. 39, no. 2, pp. 87–96, 1987.

[9]   A. Driesse, W. Zaaiman, D. Riley, N. Taylor, and Stein J.S., "Indoor and outdoor evaluation of global irradiance sensors," *31st European Photovoltaic Solar Energy Conference and Exhibition*, Hamburg, Germany, 2015.

[10]   Mencke & Tegtmeyer GmbH, *Quick Reference Guide for Analog Silicon Irradiance Sensors.* [Online] Available: https://www.imt-solar.com/fileadmin/docs/en/products/Si_Instruction_analog_E.pdf.

[11]   Mencke & Tegtmeyer GmbH, *Silicon Irradiance Sensor Technical Data.* [Online] Available: https://www.imt-solar.com/fileadmin/docs/en/products/Si-Sensor_2017_E.pdf.

[12]   PVSyst SA., "Project design- PVSyst: Array incidence loss (IAM)," [Online] Available: https://www.pvsyst.com/help/index.html?iam_loss.htm.

[13]   S. Grünsteidl, P. Borowski, and T. Dalibor, "Evaluation of irradiance sensor technologies for plant monitoring of PV systems with CIGS thin film modules," *35th European Photovoltaic Solar Energy Conference and Exhibition*, pp. 2021–2027, Brussels, 2018.

[14]   K. Bothe and D. Hinken, "Calibration of Solar Irradiance Sensors," [Online] Available: https://isfh.de/en/dienstleistungen/isfh-caltec/strahlungssensoren/.

[15]   A. Habte, M. Sengupta, A. Andreas, S. Wilcox, and T. Stoffel, "Evaluating Solar Resource Data Obtained from Multiple Radiometers Deployed at the National Renewable Energy Laboratory," (eng), *29th European Photovoltaic Solar Energy Conference and Exhibition*, pp. 2892–2899, Amsterdam, 2014.

[16] D. E. Guzman Razo, S. Killinger, B. Müller, and
      C. Wittwer, "A Comparison of Two Models for the
      Separation of Direct and Diffuse Irradiance in
      Plane of Array," (en), 2019.